In-silico modelling of fullerene and fullerene adsorbed by nO$_2$ molecules (n(O$_2$)@C_m with n = 1, 2, 4 and m = 48 and 60) as potential SARS-CoV-2 inhibitors

MEZIANE BRAHIMI[1],*, DJAMILA SELLAM[2], AFAF BOUCHOUCHA[3], YASSAMINA ARBIA[1], HADJER MERAZKA[3], RADIA BAGTACHE[4], KHALED DJEBBARI[1], KHALDOUN BACHARI[5] and OUALID TALHI[5]

[1]Laboratoire de Physico Chimie Théorique et Chimie Informatique (LPCTCI), USTHB, BP N° 32 Al Alia, 16111 Alger, Algeria
[2]Laboratoire de Chimie Appliquée et de Génie Chimique, Université Mouloud Mammeri, 15000 Tizi Ouzou, Algeria
[3]Laboratoire d'Hydrométallurgie et Chimie Inorganique Moléculaire, USTHB, BP N° 32 el Alia, 16111 Alger, Algeria
[4]Laboratoire de Chimie Organique Appliquée, USTHB, BP N° 32 el Alia, 16111 Alger, Algeria
[5]Centre de Recherche en Analyses Physico Chimiques (CRAPC), 42415 Bou Ismail, Tipaza, Algeria
*Author for correspondence (mez_brahimi@yahoo.fr; m.brahimi@usthb.dz)

Abstract. COVID-19 pandemic started more than a year ago and has infected more than 115 million of people from $\sim$210 countries and >2.5 million of deaths worldwide being reported without any commercial and effective treatment or vaccine being yet released. However, recent studies on nanomaterials such as fullerenes, carbon nanotubes and graphene showed that they possess anti-inflammatory, antiviral, anti-oxidant and anti-HIV properties. Herein, the interactions which established between the fullerenes C_m (m = 48, 60, 70, 80, 84 and 86) and the spike protein (SP) of SARS-CoV-2 and the human ACE2 receptor have been investigated based on the density functional theory (DFT) method with the CAM-B3LYP functional and the 6-31G* basis. The results of this study show that C48 exhibited as potential inhibitor of SARS-CoV-2. Because of the presence of heteroatoms on the surface of fullerenes which systematically reduce energy gaps, which in turn increase their reactivities. The oxygen adsorbed by fullerenes increases the number of non-covalent contacts and involves a large number of hydrogen bonds, while decreasing the binding energies. Thus, the hACE2-SP-4O$_2$@C60 complex is strongly recommended for inhibiting SARS-CoV-2 in the final phase of contamination.

Keywords. Fullerenes; fullerene adsorbed by nO$_2$; SARS-CoV-2; DFT; molecular docking.

1. Introduction

C60 is the first member of the fullerene family to be synthesized. It contains only carbon atoms with 60π electrons which are not completely delocalized due to its crystallographic structure [1]. Indeed, the C60 has a truncated icosahedrons structure with 32 faces, including 20 hexagons and 12 pentagons, each of these being surrounded by six hexagons.

The crystallographic structure reveals that the C–C bond lengths in the pentagons are identical and equal to 1.45 Å which is characteristic of a single Csp^3–Csp^3 type, while in the hexagons, the bond lengths are alternately of 1.45 Å (single bond) which are common to a pentagon and a hexagon and 1.38 Å (double bonds) which are common to two hexagons. The localization of π electrons would make the carbon atoms in the C60 non-identical,

leading to a different possibility of interactions. This could suggest that C_m (m = 48, 60, 70, 80, 84 and 86) would be a potential candidate for inhibition of SARS-CoV-2.

It has been more than a year since the COVID-19 [2] pandemic has spread in the world with an upsurge in the number of infected people that exceeds 115 million worldwide with >2.5 million of deaths without any treatment or effective vaccine being proposed until now. To propose those which inhibit the SARS-CoV-2 and based on the databases of molecules, several molecular docking studies have been carried out. Nanomaterials, such as fullerenes, nanotubes and graphene have been shown to interact strongly with peptide and protein assemblies [3,4] and have antiviral [5–11], anti-oxidant, anti-inflammatory [12] and anti-HIV [9] properties. The use of fullerenes in medicine is increasingly explored even if several studies

warn of potential damage caused to the living organisms [13,14] and even *in-vivo* studies have shown that the C60 and its derivatives are not toxic [15,16]. It would be necessary to understand in advance, the interactions that are established between fullerenes and the spike protein (SP) as well as with the human angiotensin-converting enzyme 2 (hACE2). On the other hand, it has been showed that in agreement with the experience that C60 binds strongly with Aβ fibrils and the binding energy decreases with increase in the size of fullerenes [17]. In addition, one of the main characteristics of the C60 is its ability to capture free radicals that protects biological systems from cell destruction [18,19]. The presence of several double bonds is responsible for scavenging free radicals [20] and probably for establishing strong non-covalent interactions between fullerenes and the various residues of the spike protein and the hACE2 receptor. Moreover, it has been showed that the hydroxychloroquine [21] and adsorption of chloroquine on C60 fullerenes and the doped one with B, Al and Si are thermodynamically stable [22] and are potential carriers of drugs [23–25].

For all these reasons and in the absence of treatment for the COVID-19 pandemic, the fullerenes can be an approach to be exploited [17], which means it is interesting to study the interactions between the nanomaterials in the different sites of the contact area (figure 1) between SARS-CoV-2 and the hACE2 receptor. Furthermore, a recent experimental [26] study showed that the lipid layer present in the virus of COVID-19 can be deactivated by the nanocarbon-coated surfaces, such as fullerenes. Other studies showed anti-cancer effects of fullerene derivatives [27–29]. Herein, our work reports the exploitation of the electronic and structural characteristics of fullerenes and the examination of their interactions with the spike protein and hACE2 receptor.

For this purpose, we use the density functional theory (DFT) method with the CAM-B3LYP functional and the 6-31G* basis sets for the determination of most

Figure 1. Interaction interface between spike protein and human ACE2 receptor.

stable structures of the different ligands (C_m, m = 48, 60, 70, 80, 84 and 86) and fullerenes adsorbing oxygen molecules $C_m@nO_2$ [30] without any symmetry constraint. Chimera 1.14 [31] software is used to perform molecular docking. We use the cleaned PDB files (6LZG and 6MOJ) (figure 1), from the databank from which we extracted the structures of the spike protein and hACE2 receptor.

2.   Computational details

Fullerenes C48(D_{6d}), C60(I_h), C70(D_{5h}) and C80(C_{2v}) have been optimized without any symmetry constraint at the DFT levels using the CAM-B3LYP functional [32–34] and the split valance polarized basis set 6-31G* implemented in Gaussian 03 [35]. The PDB file of SARS-CoV-2 spike protein (SP) RBD-hACE2 complex (PDB ID 6LZG or 6MOJ) was obtained from the structural bioinformatics (RCSB) protein data bank (PDB) (http://www.rcsb.org/structure/6LZG). We have used the UCSF Chimera 1.14 [31] to highlight the structure of the ligand and/or protein-complex structure, to perform the various functions associated with ligand and protein preparations and acting as an interface to enable molecular docking calculations using locally hosted AutoDock Vina software [36]. Prior to molecular docking, the hACE2 protein (part A) and S-protein (part B) in 6LZG PDB files were deleted from the PDB file of the complex, respectively, to study the S-protein-fullerene (SP@C_m) and hACE2-fullerene (hACE2@C_m) complexes. In addition, all non-standard residues including that of water were also removed. The structure of each fullerene ligand has been incorporated into UCSF Chimera [31] using the optimized structure at the CAM-B3LYP/6-31G* levels, which also have been imported in the PDB file format obtained from Gaussian 03 software calculation at B3LYP/6-31G* levels [35] and visualized by GaussView 5.0.9 package [37]. The PDBQT files of the S-protein RBD and fullerene ligands were generated after adding all hydrogen and charges to each structure. The S-protein and hACE2 docking search box were assigned by varying the receptor search volume in terms of size and centre to cover the contact area previously observed between the S-protein RBD and hACE2 receptor. The number of binding modes was fixed to 10 with exhaustiveness of search set to eight. The maximum energy difference was fixed up to 3 kcal mol^{-1}. The obtained molecular docking results were then aligned with the PDBQT files of the S-protein, hACE2 and S-protein RBD-hACE2 complex to emphasize the interaction type of docked complexes in the S-protein, hACE2 and S-protein-hACE2 binding interface, respectively. The AMBER ff14SB force field was used [38].
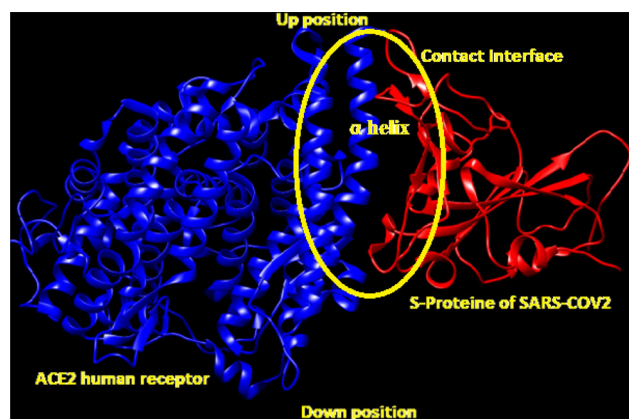
3. Results and discussion

3.1 *Structural studies of different ligands*

The results giving the 3D optimized geometries of different fullerenes (C_m, figure 2a) and different fullerenes adsorbed by nO_2 molecules $nO_2@C_m$ (figure 2b) are illustrated in figure 2. The calculations, for the energy minima, lead to normal modes of vibration which are all real. Overall, when fullerene size increases, the energy gap decreases, so the reactivity increases.
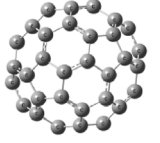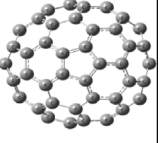
The studies of the physicochemical descriptors [39]:

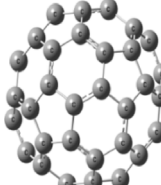$$I = - E_{HOMO};\ A = -E_{LUMO};\ \mu = -\frac{1}{2}(I+A) = -\chi_M;\ \eta = \frac{1}{2}(I-A);$$
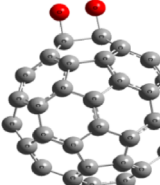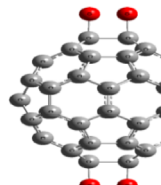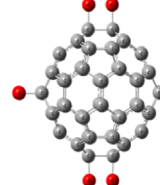
$$\sigma = \frac{1}{\eta};\ \omega = \frac{\mu^2}{2\eta};\ v = -I$$

where χ_M is the Mulliken electronegativity, I the ionization potential, A the electron affinity, μ the chemical potential, η the chemical hardness, ω the electrophylicity and v the nucleophilicity, which are calculated at the CAM–B3LYP/6-31G* level with the Koopmans

(a)

(eV)	C48(D$_{6d}$)	C60(I$_h$)	C70(D$_{5h}$)	C80(C$_{2v}$)
I = - E$_{HOMO}$	5.678	5.987	5.921	5.908
A = - E$_{LUMO}$	3.805	3.224	3.236	4.301
Gap	1.873	2.763	2.685	1.607
μ	-4.742	-4.606	-4.579	-5.105
η	0.937	1.382	1.345	0.804
ω	12.006	7.676	7.809	16.217
Nu	-5.678	5.987	-5.921	-5.908
V(Å^3)	461.3	498.0	591.3	690.0

(b)

(eV)	C60	C60@O$_2$	C60@2O$_2$	C60@4O$_2$
I = - E$_{HOMO}$	5.987	6.023	6.105	6.340
A = - E$_{LUMO}$	3.224	3.419	3.588	3.795
Gap	2.763	2.604	2.517	2.545
μ	-4.606	-4.721	-4.847	-5.068
η	1.382	1.302	1.259	1.273
ω	7.676	8.559	9.330	10.088
Nu	-5.987	-6.023	-6.105	-6.349

Figure 2. (**a**) Optimized structure of C48(D$_{6d}$), C60(I$_h$), C70(D$_{5h}$), C80(C$_{2v}$) and (**b**) C60, C60@O$_2$, C60@2O$_2$ and C60@4O$_2$ obtained at the CAM–B3LYP/6-31G* levels with ionization potential I, electron affinity A, energy gap, chemical potential μ, chemical hardness η, electrophilicity ω, nucleophilicity v in eV and molecular volume in Å^3 evaluated by Chimera software.

approximation [40], show that the C60@nO$_2$ complexes with fullerene are more reactive than the C60. In fact, energy gap, electrophilicity ω, e chemical potential μ, electronegativity χ ($-\mu$) and nucleophilicity v increase in absolute values in all cases when we go from C60 to complexes.

The IR spectra given in figure 3, show the normal mode of vibration calculated at the CAM-B3LYP/6-31G* level where the IR peak half-width at half-height is multiplied by 40 cm^{-1}.

From the IR spectra (figure 3), the band appearing around 588 cm^{-1} for C60 disappears as the number of adsorbed oxygen molecules increase; it completely disappears for the C60@4O$_2$ complex. It is the same for the bands that appear between 1214 and 1460 cm^{-1}.

A new band, large and intense, characteristic of oxygenated compound: C–O elongations symmetrical (v_{C-O}^{Sym}) at 1070 cm^{-1} and asymmetric (v_{C-O}^{aSym}) at 1170 cm^{-1} appear for the fullerene complexes. The vibration spectra of all other C_m@nO$_2$ complexes with m = 48, 70, and 80 with n = 1, 2 and 4 lead to the same conclusions.

The calculated area under the curve (AUC) of the characteristic peak at 1000–1200 cm^{-1} of adsorbed, as function of the number of adsorbed oxygen molecules nO$_2$, is shown in figure 4. We note that the surface increases linearly with the number nO$_2$. This result confirms the fixation and the quantities of oxygen adsorbed.

From the frontier molecular orbital (FMO), a clear reduction in the energy gap (figure 2b) is observed which is corresponding to a greater reactivity. The shape of the
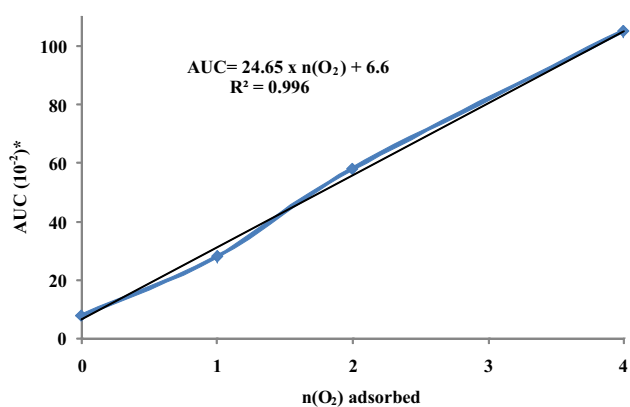

Figure 4. Area under the curve (AUC $\times$ 10^{-2}) of (*) IR spectra between 1000 and 1200 cm^{-1} *vs.* n(O$_2$) adsorbed.

FMOs, given in figure 5, shows a different distribution of the C60@nO$_2$ complexes.

3.2 *Docking results*

3.2a *Fullerene ligand*: Taking into account the contact interface between the spike protein of SARS-CoV-2 and the hACE2 (figure 1), we have opted for all the docking calculations with the size of the box modelling in this interface, such as special parameters: centre: -33.57; 32.45; 1.938 and x = 22.0; y = 45.0 and z = 20.0.

The results of the SP@C_m and hACE2@C_m complexes, shown in table 1, highlight the following:
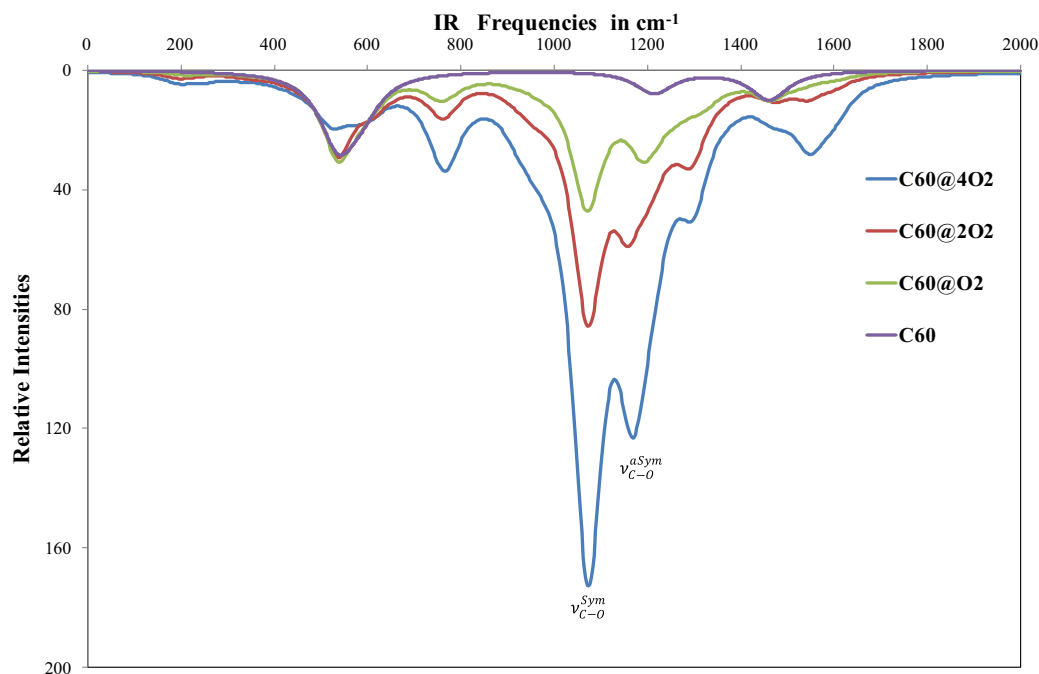
Figure 3. IR spectra of C60 and C60@nO$_2$ with n = 1, 2 and 4 obtained at CAM-B3LYP/6-31G* levels.
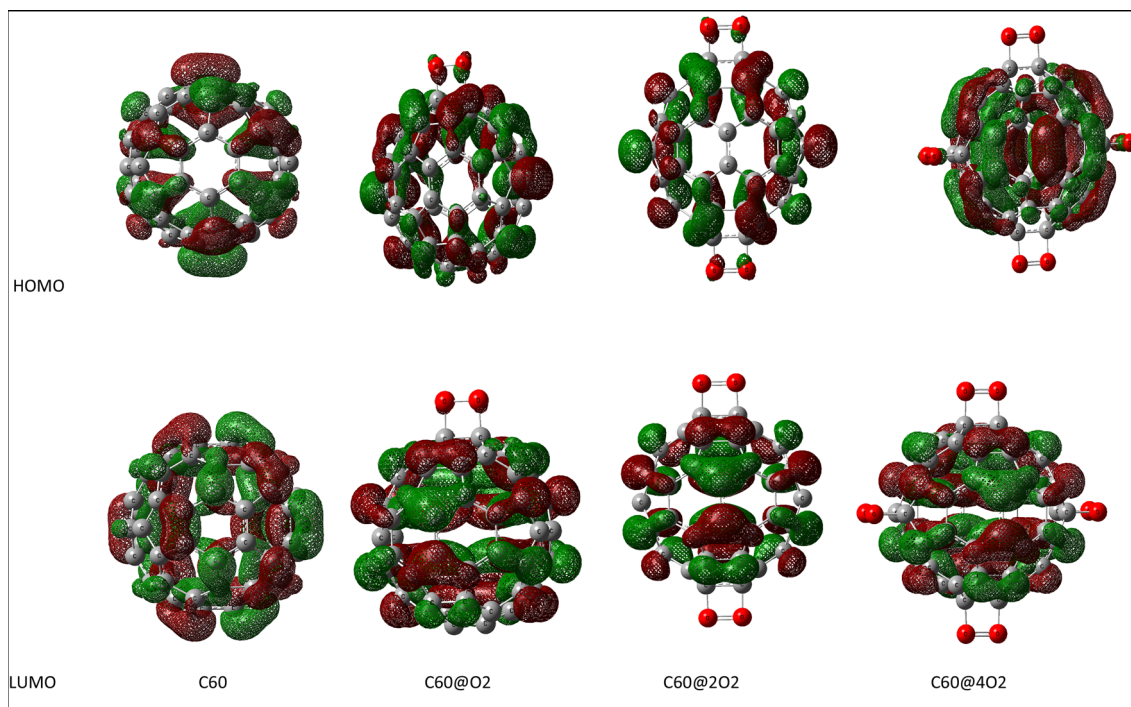
Figure 5. FMO of C60, C60@O$_2$, C60@2O$_2$ and C60@4O$_2$ obtained at CAM-B3LYP/6-31G* level.

Table 1. Binding energy intervals (kcal mol^{-1}) of the first 10 most stable states of Cible@fullerene complex.

Cible@fullerene type	Binding energy intervals between:	RMSD between:
SP@C48	−8.0 to −8.0	0.00 to 0.07
SP@C60	−7.8 to −7.8	0.00 to 0.07
SP@C70	−8.1 to −7.9	0.00 to 0.76
SP@C80	−8.5 to −8.2	0.00 to 0.84
SP@C84	−8.3 to −8.2	0.00 to 0.76
SP@C86	−8.6 to −8.3	0.00 to 0.80
hACE2@C48	−10.2 to −9.0	0.00 to 1.47
hACE2@C60	−7.9 to −7.9	0.00 to 0.11
hACE2@C70	−9.0 to −8.8	0.00 to 0.64
hACE2@C80	−9.1 to −8.9	0.00 to 0.82
hACE2@C84	−9.0 to −8.8	0.00 to 0.75
hACE2@C86	−9.4 to −9.0	0.00 to 0.81
hACE2@SP@C48	−8.5 to −7.8	0.00 to 12.22
hACE2@SP@C60	−5.1 to −5.0	0.00 to 0.16
hACE2@SP@C70	−5.2 to −4.8	0.00 to 0.62
hACE2@SP@C80	−2.5 to +0.2	0.00 to 0.76
hACE2@SP@C86	0.0 to 1.0	0.00 to 0.82

(i) The interaction energies are non-covalent types.

(ii) Overall, the binding energy decreases with increase in the sizes of the fullerene. This trend is not observed for C48 and C84, this exception is due to the flattened shape of the structure that promotes better contacts with the target as discussed further.

The same findings also apply for complexes hACE2@C_m (m = 48, 60, 70, 80, 84 and 86) (table 1). Indeed, when the shape of the fullerene is oval or flattened, the corresponding binding energy is lower with more non-covalent contacts between the spike protein and hACE2 targets and ligand.

From the different interactions established (table 2), it appears that:

(i) The residues of the spike protein involved are identical from fullerene C48 to C86. C48 established 48 interactions

Table 2. Residues involved in the different contacts established in Cible@C_m (m = 48, 60, 70, 80, 84 and 86).

| Cible@C_m	Number of non-covalent interactions	Residues involved
SP@C48	48	GLN493, GLY496, TYR449, TYR505 and GLN498
SP@C60	25	GLN493, GLY496, TYR449, TYR505 and GLN498
SP@C70	25	GLN493, GLY496, TYR449, TYR505 and GLN498
SP@C80	32	GLN493, GLY496, TYR449, TYR505 and GLN498
SP@C84	31	GLN493, GLY496, TYR449, TYR505 and GLN498
SP@C86	34	GLN493, GLY496, TYR449, TYR505 and GLN498
hACE2@C48	64	GLN96(05), LYS26(11), VAL93(11), ASP30(16), ASN33(08), THR92(01) and PRO389(12)
hACE2@C60	25	PHE28(6), LYS31(9), LEU79(2) and TYR83(8)
hACE2@C70	33	THR27(4), PHE28(5), LYS31(12), LEU79(6) and TYR83(6)
hACE2@C80	31	THR27(3), PHE28(6), LYS31(12), LEU79(5) and TYR83(5)
hACE2@C84	27	THR27(5), PHE28(5), LYS31(10), LEU79(2) and TYR83(5)
hACE2@C86	32	THR27(5), PHE28(7), LYS31(8), LEU79(7) and TYR83(5)
hACE2@SP@C48	86	ARG403(18), LYS417(17), PRO389(17), ASN33(9), ASP30(4), HIS34(10), TYR505(2), ARG393(5), GLN388(2) and ALA387(2)
hACE2@SP@C70	26	GLN474(8), SER19(7), LYS458(9) and GLY476(2)
hACE2@SP@C80	32	GLN474(13), SER19(11), LYS458(4) GLY476(2) and SER477(1)
hACE2@SP@C86	57	SER19(25), GLN474(15), GLY476(4), LYS458(6) and SER477(6)
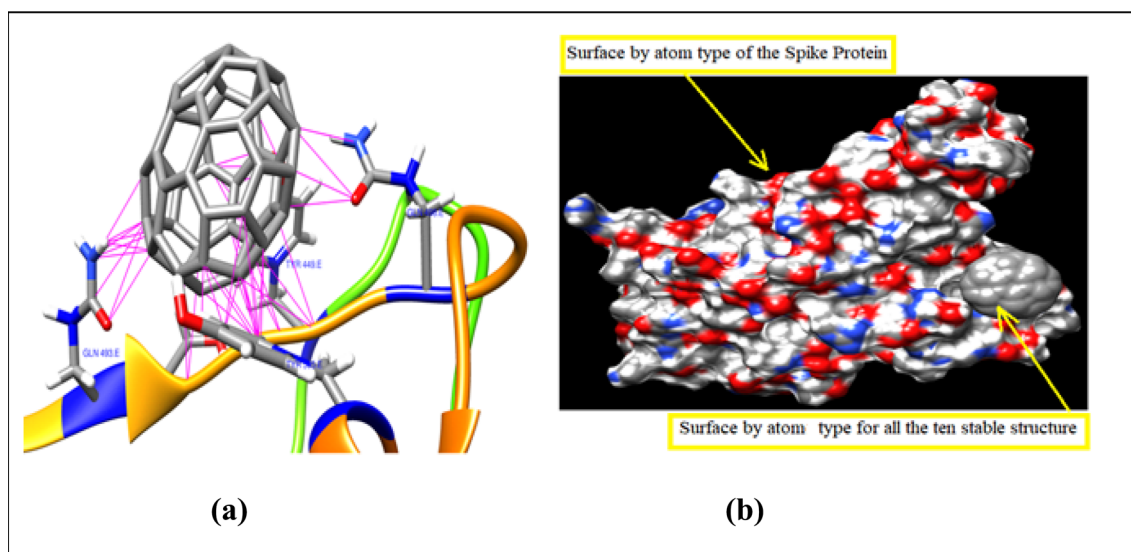
Figure 6. (**a**) Different contacts with the C48 fullerene and the spike protein. (**b**) Surface by atom type for all 10 stable structures of SP@C48 complexes.

due to its flattened shape with a binding energy of −8.0 kcal mol^{-1} (figure 6a). All 10 stable structures are located at down position of the spike protein (figure 6b). However, for C86 form 34 contacts with a binding energy of −8.6 kcal mol^{-1}. The order of magnitude of the binding energies is a neighbour, but C48 would link better to the spike protein.

(ii) The residues involved in hACE2@C_m are also identical in all cases implicating the same conclusion as above. Even if the lowest binding energy corresponds to the hACE2@C86 complex (−9.4 kcal mol^{-1}, table 1), the advantage of the contacts is in favour of the hACE2@ complex C48 (binding energy of −8.4 kcal mol^{-1}, figure 7a

and b) with 53 contacts which correspond to the following residues: THR27(13), PHE28(9), LYS3(13), LEU79(12) and TYR83(6) (in brackets the number of contacts per residue).

(iii) For the complexes hACE2@SP@C_m type (m = 48, 60, 70, 80, 84 and 86), the advantage is also attributed for the smaller fullerene sizes (C48) with a binding energy of −8.5 kcal mol^{-1} and 86 interactions distributed as follows: ARG403(18, SP), LYS417(17, SP), PRO389(17, hACE2), ASN33(9, hACE2), ASP30(4, hACE2), HIS34(10, SP), TYR505(2, SP), ARG393(5, SP), GLN388(2, hACE2) and ALA387(2, hACE2); including 52 contacts with the spike
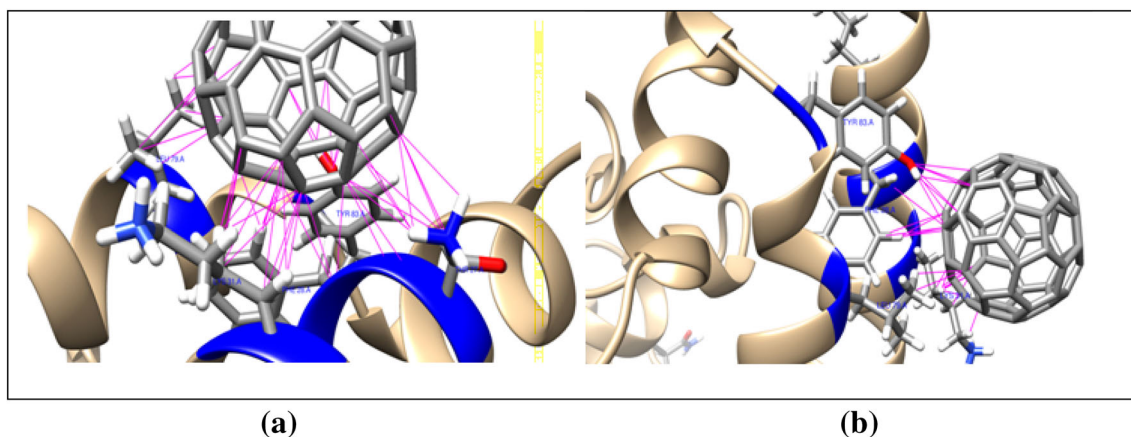
Figure 7. Different contacts with the (**a**) more and (**b**) second stable hACE2@C48 complex.
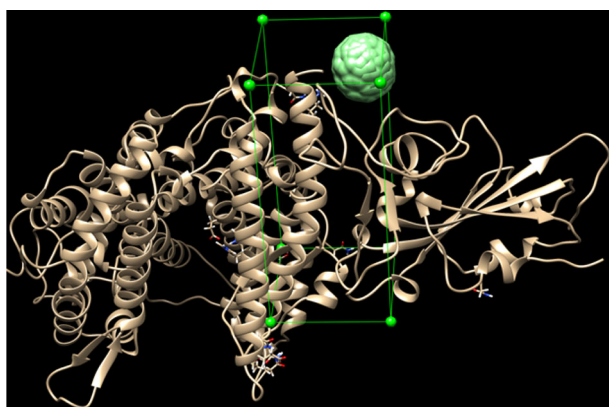
Figure 8. Docking positions of the 10 stable complexes formed by spike protein-hACE2 with these C_m (m = 70, 80, 84 and 86) fullerenes.

protein and 34 with the hACE2 receptor. While for the other fullerenes, considering their molecular volume (figure 2), their binding energies and the number of contacts they established (tables 1 and 2), they cannot be inhibitors of SARS-CoV-2 because they linked outside of the contact area between the spike protein and the hACE2 receptor (figure 8).

The different interactions of both stable conformations are represented in figure 7a and b.
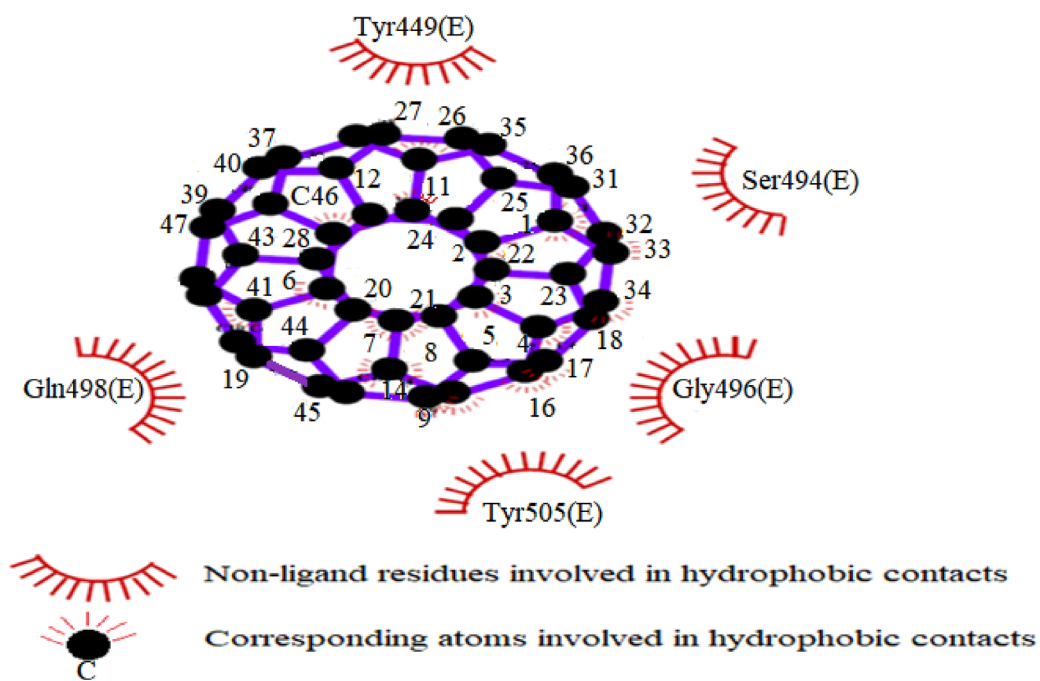
Figure 9 shows the hydrophobic contacts between SER494, GLY496, TYR449, TYR505 and GLN498 residues of the spike protein and the corresponding atoms of the ligand obtained with the LigPlot$^+$ v.2.2 multiple ligand–protein interaction diagrams of drug discovery [41].

Figure 10 shows, in 2D, the 64 hydrophobic contacts between GLN96, LYS26, VAL93, ASP30, ASN33, THR92 and PRO389 residues of the ACE2 receptor and corresponding atoms of ligand.

3.2b *Complex C_m@nO_2 ligand*: SARS-CoV-2 is found to cause several and very different symptoms, such as hypoxemia (lack of oxygen). Once the cell is infected with

SARS-CoV-2, it depletes the cell in oxygen. It is known that fullerenes adsorb oxygen molecules and the presence of heteroatoms on them systematically reduces the energy gap, this means that the exchange of electrons is greater and become most reactive compared to pure fullerenes [42,43]. The presence of oxygen atoms on the surface of fullerenes will promote the formation of hydrogen bonds with various targets (spike protein and hACE2), which will strengthen the binding of modified fullerenes to these targets and thus inhibit the penetration of SARS-CoV-2 inside the cell. For these reasons, we have optimized at the CAM-B3LYP/6-31G* level, without symmetry constraints for the complexes: C_m@nO_2 (n = 1, 2 and 4 and m = 48, 60 and 80) (table 3). PDB files were created using GaussView 5.0.9 and transferred to Chimera 1.14 software where molecular docking was performed by studying their interactions with the spike protein and hACE2.

The adsorption of oxygen by the various fullerenes decreases the values of the binding energy (see figure 2b) and increases the number of contacts by including stabilizing interactions through the formation of hydrogen bonds, e.g., the SP-C48@$2O_2$ has a binding energy of -9.1 kcal mol^{-1} with 43 contacts whose five-hydrogen bonding, compared to that of SP-C48 complex which is of -8.0 kcal mol^{-1} with 48 non-covalent contacts without any hydrogen bond. On the other side, the SP-C80 complex has a binding energy of -8.5 kcal mol^{-1} with 32 non-covalent contacts, while that of the SP-C80@$4O_2$ complex is -10.7 kcal mol^{-1} with 42 contacts including seven hydrogen bonds, i.e., a difference of 2.2 kcal mol^{-1} is in favour of the stability of the SP-C80@$4O_2$ complex, especially, since all the contacts are established inside the spike protein–hACE2 interface. In all cases, the adsorption of oxygen on the fullerenes promotes the binding of the ligand to the spike protein and to the hACE2 receptor with a difference in stabilizing binding energy of around 1.2 kcal mol^{-1} with a great number of contacts including hydrogen bonds. The most favourable case is the hACE2-SP-C60@$4O_2$ complex

Figure 9. Hydrophobic contacts between the residues of the spike protein (table 2) and corresponding atoms of the C48 ligand.
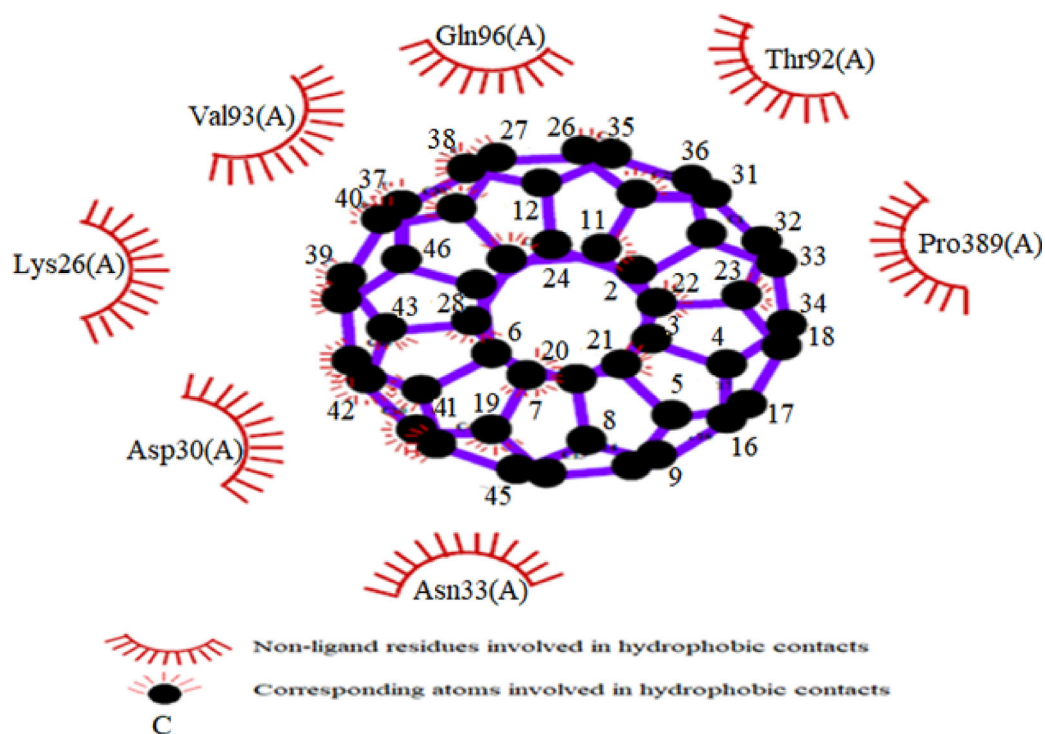

Figure 10. Hydrophobic contacts between the residues of the ACE2 receptor (table 2) and corresponding atoms of the C48 ligand.

Table 3. Binding energy intervals (kcal mol^{-1}), RMSD (Å) intervals for the top ten stable structures and contacts number in the 10 stable cible@nO$_2$ complexes.

Cible@fullerene-adsorbed type	Binding energy intervals between:	RMSD between:	Number of contacts for the most stable complex of the lowest binding energy
SP-C48@2O$_2$	−9.1 to −8.7	0.00 to 1.77	43 (5 H bonds)*
SP-C60@2O$_2$	−8.7 to −8.5	0.00 to 1.24	25 (3 H bonds)
SP-C60@2O$_2$	−8.7 to −8.6	0.00 to 1.70	24 (3 H bonds)
SP-C60@4O$_2$	−9.7 to −9.2	0.00 to 1.84	35 (5 H bonds)
SP-C60@8O$_2$	−10.7 to −10.1	0.00 to 1.68	42 (7 H bonds)
hACE2-C60@4O$_2$	−9.1 to −8.8	0.00 to 1.66	33 (2 H bonds)
hACE2-C80@4O$_2$	−6.5 to −5.9	0.00 to 1.67	39 (4 H bonds)
hACE2-SP-C60@4O$_2$	−13.2 to −12.7	0.00 to 1.06	49 (18 H bonds)

*In parentheses are given the number of hydrogen bond contacts established for the 10 most stable conformations.
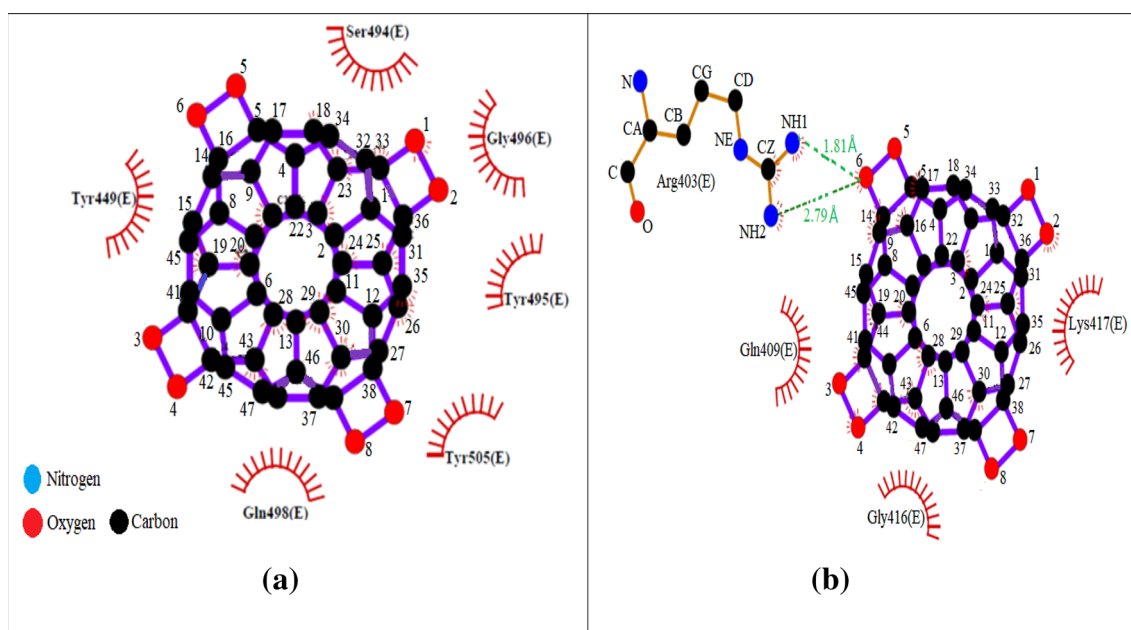
**Figure 11.** (a) Hydrophobic contacts and (b) hydrogen bond in the C48@4O$_2$ complex.

with a binding energy of −13.2 kcal mol^{-1} compared to the hACE2-SP-C60 complex with a binding energy of −5.1 kcal mol^{-1}. Once the spike protein is attached to the hACE2 receptor, that is to say, in the final phase of contamination, the hACE2-SP-C60@4O$_2$ complex is strongly recommended to inhibit the action of SARS-CoV-2; the difference in binding energy is of −8.1 kcal mol^{-1} with 18 hydrogen bonds (with the 10 stable structures) that form with the complex where four oxygen molecules are adsorbed on the C60.

For example, for the most stable conformation of C48@4O$_2$, three hydrogen bonds are formed, two between ARG403 (2.79 and 1.81 Å) and oxygen O$_6$ (figure 6a) where the third did not appear (complexity of 2D representation), is established between the TYR505 and O$_7$ (figure 11a) which is 2.51 Å (figure 11b).

3.2c *H$_2$O solvent effect*: Water as a solvent is a capital importance, if we research stabilizing interaction between the different targets and the adsorbed fullerenes. The study of solvent effect has not been investigated in this work because of two considerations:

(i) Adsorbed fullerenes can be used as a layer covering protective masks to trap SARS-CoV-2 because of this solid physical state. So, considering the effect of solvent is unnecessary in this case.

(ii) If the adsorbed fullerenes are administrated, the effect of solvent (water) increases the contact area between the targets and the ligands, and therefore, the stabilizing interactions would be greater. In fact, the successive layers of water molecules which are linked to the adsorbed fullerenes would be formed by hydrogen bonds as shown in figure 12.
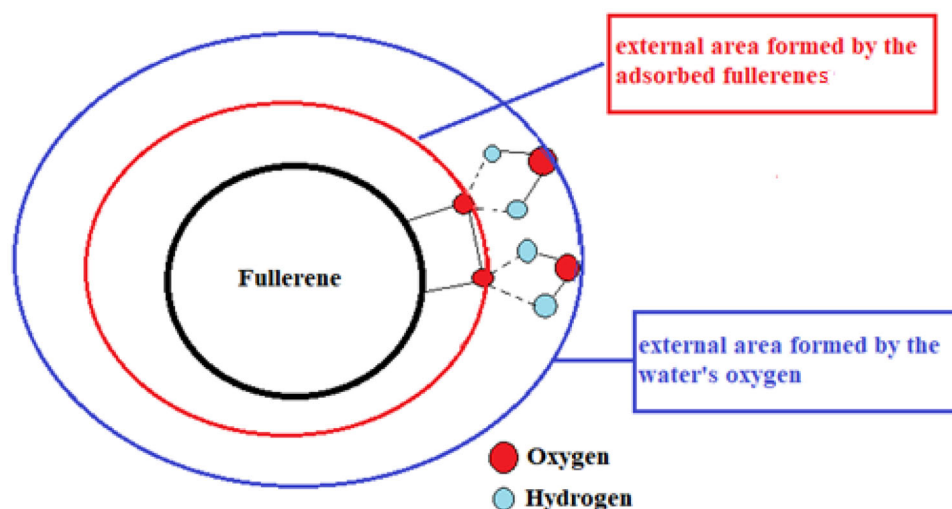
Figure 12. Schematic representation of the first solvation layer with H_2O.

Therefore, the contact area is identical without or with solvent.

4. Conclusion

From this study, it emerges that fullerenes are potential inhibitors of SARS-CoV-2 because of the number of interactions which are established with the spike protein and the hACE2 receptor, respectively. C48 presents as the best asset due to its flattened shape which allows it to have a greater inhibitory surface at the contact interface between the spike protein and the hACE2 receptor. The adsorption of oxygen molecules on various fullerenes increases the non-covalent contacts and creates a new interaction with hydrogen bonds which stabilize the various complexes, such as SP-C_m@nO$_2$, ACE2-C_m@nO$_2$ and ACE2-SP-C_m@nO$_2$. In the final phase of contamination, the hACE2-SP-C60@4O$_2$ complex is strongly recommended to inhibit the action of SARS-CoV-2 because of its binding energy and the large number of hydrogen bond interactions.

Acknowledgements

References

[1] Kroto H W, Heath J R, O'Brien S C, Curl R F and Smalley R E 1985 *Nature* **318** 162

[2] Gupta V 2020 *Lett. Appl. NanoBioScience* **9** 1083

[3] Sivasankarapillai V S, Pillai A M, Rahdar A, Sobha A P, Sachi Das S, Mitropoulos A C *et al* 2020 *Nanomaterials* **10** 852

[4] Li C and Mezzenga R 2013 *Nanoscale* **5** 6207

[5] El Haes H, Saleh N A, Omar A and Ibrahim M 2014 *J. Comput. Theor. Nanosci.* **11** 2136

[6] Hammed A J, Ibrahim M and El Haes H 2007 *J. Mol. Struct. Theochem.* **809** 131

[7] Saleh N A, El Haes H, Osman O, Mahmoud A A and Ibrahim M 2015 *Open Spectrosc. J.* **9** 1

[8] Liliana I, Nosik N N and Kondrashina N G 2016 *Int. J. Infect. Dis.* **53** 82

[9] Nosik D N, Lialina I K, Kalnina L B, Lobach O A, Chataeva M S and Rasnetsov L D 2009 *Vopr. Virusol.* **54** 41

[10] Innocenzi P and Stagi L 2020 *Chem. Sci.* **11** 6606

[11] Suku A S, Jayakumar A and Valappil M P 2020 *Lett. Appl. NanoBioScience* **9** 1637

[12] Klimova R, Andreev S, Momotyuk E, Demidova N, Federova N, Chernoryzh Y *et al* 2020 *Fuller. Nanotub. Carbon Nanostruct.* **28** 487

[13] Kayat J, Gajbhiye V, Tekade R K and Jain N K 2011 *Nanomedicine* **7** 40

[14] Yang S T, Liu Y, Wang Y W and Cao A 2013 *Nano. Micro Small* **9** 1635

[15] Moussa F, Trivin F, Ceolin R, Hadchouel M, Sizaret P Y, Greugny V *et al* 1996 *J. Fuller. Sci. Technol.* **4** 21

[16] Bobylev A G, Okuneva A D, Bobyleva L G, Fadeeva I S, Fadeev R S, Salmov N N *et al* 2014 *Biofizika* **59** 843

[17] Huy P D Q and Li M S 2014 *Phys. Chem. Chem. Phys.* **16** 20030

[18] Bakry R, Vallant R M, Najam-Ul-Haq M, Rainer M, Szabo Z, Huck C W *et al* 2007 *Int. J. Nanomed.* **2** 639

[19] Sun T and Xu Z 2006 *Bioorg. Med. Chem. Lett.* **16** 3731

[20] Goodarzi S, Da Ros T, Conde J, Sefat F and Mozafari M 2017 *Mater. Today* **20** 460

[21] Dubey D 2020 *Lett. Appl. NanoBioScience* **9** 1705

[22] BagheriNovir S and Reza Aram M 2020 *Chem. Phys. Lett.* **757** 137869

[23] Kuznietsova H, Dziubenko N, Herheliuk T, Prylutskyy Y, Tauscher E, Ritter U *et al* 2020 *Pharmaceutics* **12** 794

[24] Nalepa P, Gawecki R, Szewczyk G, Balin K, Dulski M, Sajewicz M *et al* 2020 *Cancer Nano.* **11** 2

[25] Huang H J, Kraevaya O A, Voronov I, Troshin P A and Hsu S H 2020 *Int. J. Nanomed.* **15** 20486

[26] Siddiquie R Y, Agrawal A and Joshi S 2020 *Trans. Indian Natl. Acad. Eng.* **5** 343

[27] Tatyanenko L V, Pokidova O V, Goryachev N S, Kraevaya O A, Khakina E A, Yu Belik A *et al* 2020 *Bull. Exp. Biol. Med.* **69** 89

[28] Xu H, Tu X, Fan G, Wang Q, Wang X and Chu X 2020 *J. Mol. Liq.* **318** 114315

[29] Bagheri Novir S and Reza Aram M 2020 *Chem. Phys. Lett.* **757** 137869

[30] Tabari L and Farmanzadeh D 2019 *Appl. Surf. Sci.* **479** 569

[31] Pettersen E F, Goddard T D, Huang C C, Couch G S, Greenblatt D M, Meng E C *et al* 2004 *J. Comput. Chem.* **25** 1605

[32] Becke A D J 1993 *Chem. Phys.* **98** 5648

[33] Lee C, Yang W and Parr R G 1988 *Phys. Rev. B* **37** 785

[34] Stephens P J, Devlin F J, Chabalowski C F and Frisch M J 1994 *J. Phys. Chem.* **98** 11623

[35] Frisch M J, Trucks G W, Schlegel H B, Scuseria G E, Robb M A, Cheeseman J R *et al* 2004 *Gaussian 03*, Revision C.02. Gaussian Inc, Wallingford, CT

[36] Trott O and Olson A J 2010 *J. Comput. Chem.* **31** 455

[37] Nielsen A B and Holder A J 2009 *Gauss View 5.0*, User's Reference. Gaussian Inc., Pittsburgh

[38] Maier J A, Martinez C, Kasavajhala K, Wickstrom L, Hauser K and Simmerling C 2015 *J. Chem. Theory Comput.* **11** 3696

[39] Makov G 1995 *J. Phys. Chem.* **99** 9337

[40] Koopmans T 1934 *Physica* **1** 104

[41] Laskowski R A and Swindells M B 2011 *J. Chem. Inf. Model.* **51** 2778

[42] Wang Y, Jiao M, Song W and Wu Z 2017 *Carbon* **114** 393

[43] Gao F, Zhao G L, Yang S and Spivey J J 2013 *J. Am. Chem. Soc.* **135** 3315